Draft version January 24, 2023
Typeset using LaTeX **twocolumn** style in AASTeX631

# Contamination in TESS light curves: The case of the Fast Yellow Pulsating Supergiants

May G. Pedersen [1,2] and Keaton J. Bell [3]

[1] *Sydney Institute for Astronomy, School of Physics, University of Sydney NSW 2006, Australia*
[2] *Kavli Institute for Theoretical Physics, Kohn Hall, University of California, Santa Barbara, CA 93106, USA*
[3] *Department of Physics, Queens College, City University of New York, Flushing, NY-11367, USA*

## ABSTRACT

Given its large plate scale of 21″ pixel$^{-1}$, analyses of data from the TESS space telescope must be wary of source confusion from blended light curves, which creates the potential to attribute observed photometric variability to the wrong astrophysical source. We explore the impact of light curve contamination on the detection of fast yellow pulsating supergiant (FYPS) stars as a case study to demonstrate the importance of confirming the source of detected signals in the TESS pixel data. While some of the FYPS signals have already been attributed to contamination from nearby eclipsing binaries, others are still suggested to be intrinsic to the supergiant stars. In this work, we carry out a detailed analysis of the TESS pixel data to attempt to fit the source locations of the dominant signals reported for 17 FYPS stars with the Python package `TESS_localize`. We are able to reproduce the detections of these signals from the TESS light curves of 14 of these sources, and we can fit reliable source locations for four. Three of these originate from contaminants, while the signal reported for BZ Tuc is likely related to its 127-day Cepheid variability. Other signals are not significant enough to be localized with our methods, or have long periods that are difficult to analyze given other TESS systematics. Since no localizable signals hold up as intrinsic pulsation frequencies of the supergiant targets, we argue that unambiguous detection of pulsational variability should be obtained before FYPS are considered a new class of pulsator.

*Keywords:* CCD photometry (208) — Time series analysis (1916) — Light curves (918) — Light curve classification (1954) — Variable stars (1761) — Photometry (1234)

## 1. INTRODUCTION

The Transiting Exoplanet Survey Satellite (TESS Ricker et al. 2014) is obtaining extensive time series photometry over most of the sky, enabling the study of photometric variability of nearly all types of astronomical objects. Interested in the behavior of massive evolved stars, Dorn-Wallenstein et al. (2019, hereafter DW19) inspected their TESS light curves for variability that could improve our understanding of these objects. In addition to apparent luminous blue variables (LBVs), unprecedented variability was identified in the TESS light curves of three yellow supergiants (YSGs). The most notable of these is HD 269953, which shows multiple periodicities.

may.pedersen@sydney.edu.au

That work was later extended, utilizing the full TESS Cycle 1 dataset to investigate variability of 76 YSGs (Dorn-Wallenstein et al. 2020, hereafter DW20). Among these, a total of five (HD 269953, HD 269110, HD 268687, HD 269840, and HD 269902) were interpreted to be rapidly pulsating on ∼day timescales, suggesting that these belong to a new class of pulsator, which were named FYPS for "fast yellow pulsating supergiants." If this is true, then FYPS would offer new exciting opportunities for studying and modelling the interiors of evolved massive stars.

Motivated by these prospects, Dorn-Wallenstein et al. (2022, hereafter DW22) set out to identify additional FYPS stars in the large and small Magellanic Clouds (LMC and SMC). The positions of their identified 17 candidate FYPS stars in the HR diagram are shown in the top panel of Fig. 1 and compared to non-rotating stellar evolution tracks of 15-35 $M_\odot$ stars of LMC com-

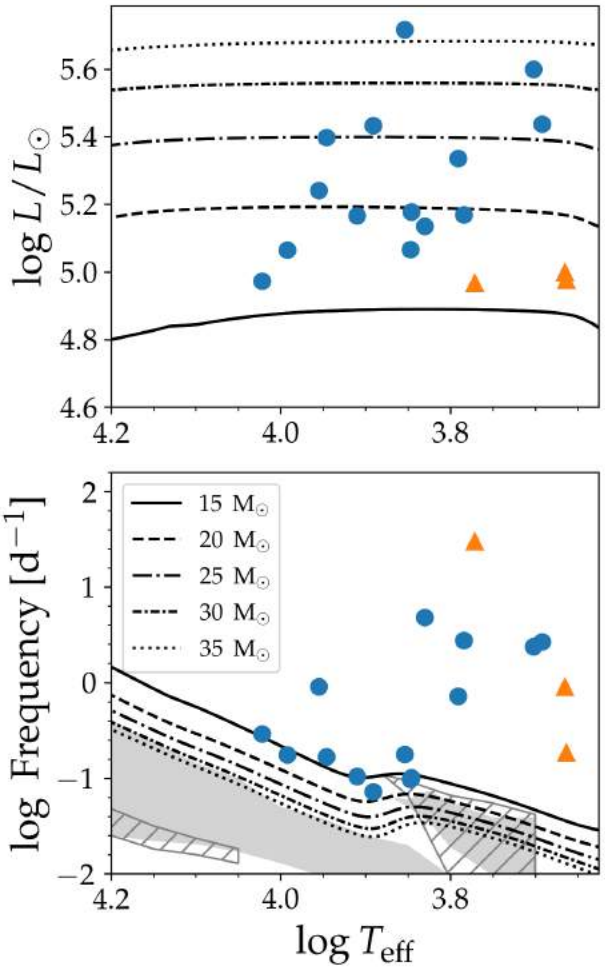


**Figure 1.** Position of the 17 FYPS stars in the HR diagram (top) and their dominant frequency $f_0$ reported by DW22 as a function of effective temperature (bottom). Blue circles indicate LMC stars, whereas orange triangles correspond to SMC stars. Example evolutionary tracks computed with `MESA` for LMC composition (see Appendix A) are shown by black lines, with the corresponding evolution of the acoustic cutoff frequency shown in the bottom panel. Different line styles correspond to different initial stellar masses as indicated by the legend. The combined predicted excited frequency ranges for a 20 and 25 $M_\odot$ star from Fig. 5 of Saio et al. (2013) at solar metallicity are shown as a function of $\log T_{\rm eff}$ for pre-RSG (hatched grey) and post-RSG (light grey) evolution, respectively.

position. The highest-amplitude signals are shown as a function of the effective temperature in the bottom panel of Fig. 1, and they are generally higher than the acoustic cutoff frequencies of the models shown by the black curves. Above this cutoff, pressure modes are no longer reflected and trapped inside the stellar interior, but become travelling waves and dissipate. Details of these calculations are provided in Appendix A. For comparison, we also show the combined predicted frequency ranges of excited modes of a 20 and 25 $M_\odot$ star derived by Saio et al. (2013) before (hatched grey) and after (light grey) the red supergiant (RSG) evolutionary stage assuming solar metallicity, which the highest-amplitude FYPS frequencies also exceed.

The work by DW22 included a renewed appreciation for possible source confusion due to blending of multiple sources in the 21″ pix$^{-1}$ TESS images. Comparing their detected frequencies to signals detected in OGLE light curves (Udalski et al. 2015) of nearby stars, they reject that several individual signals are intrinsic to the YSGs. Two of the original five FYPS stars (HD 269110 and HD 269902) were found to be contaminated as a result, along with roughly half of their initial sample of TESS variable light curves. Remaining signals that cannot be attributed to other OGLE sources are interpreted as being intrinsic to the YSGs and used to classify these objects as FYPS. The authors argue that a statistically significant excess of variable light curves extracted for stars with $\log L/L_\odot > 5$ supports that FYPS are not purely the result of contamination.

We demonstrate in this work that the TESS data themselves show additional signals for the 17 FYPS stars identified by DW22 to originate from other contaminating sources. We utilize the Python package `TESS_localize` (Higgins & Bell 2022) to fit the source locations for the strongest signals reported for these objects. Most of these signals are too weak in individual TESS sectors to be localized, but every signal that can be localized is shown to be significantly offset from the YSGs (except for BZ Tuc, which is a known long-period Cepheid variable). This includes two more of the original five stars used to define the FYPS class, HD 269953 and HD 268687. We argue that FYPS should not be considered a unique region of the pulsational H-R diagram until pulsational variability can be uniquely attributed to YSGs. This case study demonstrates the importance of using the TESS pixel data to assess potential contamination when interpreting any signals detected by TESS given its large plate scale.

## 2. THE CASE OF HD 269953 (TIC 404850274)

Expanding the sample to 17 FYPS, DW22 no longer provide the full prewhitening solutions as were in their previous papers. Instead they indicate the approximate frequency of the highest amplitude signal that they associate with each YSG, which they call $f_0$. This is after they reject signals that they are able to attribute to different OGLE sources. We detail our analysis of the prototypical FYPS star HD 269953 (TIC 404850274) here to demonstrate how we interpret their work.

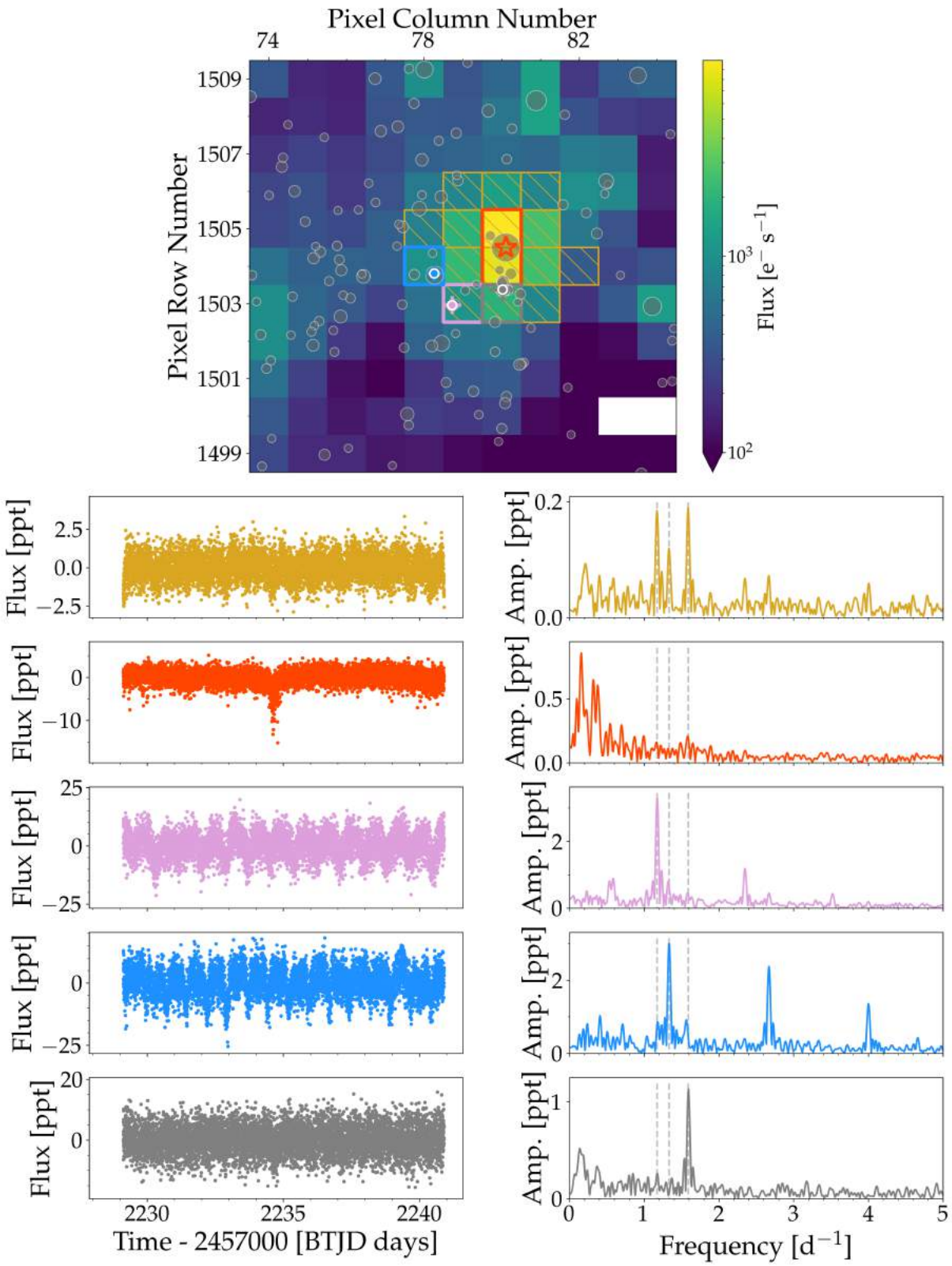


**Figure 2.** Median TPF flux of TESS sector 34 for the YSG star HD 269953 (TIC 404850274, red star) and positions of three nearby contaminating stars shown in grey, pink, and blue. Bottom panels provide the first half of each extracted light curve (left; corresponding to one spacecraft orbit) and associated periodograms (right) for the five different pixel masks indicated in the top panel. The frequency values of the three independent signals identified by DW20 based on the SPOC light curves (yellow) are shown by vertical dashed lines in the periodograms. See text for further details.

HD 269953 was one of the first YSGs found to show pulsational FYPS variability, with DW19 reporting 14 frequencies of variation. It is unclear why only four frequencies are reported in DW20: 1.593, 1.174, 1.335, and $2.671\,\mathrm{d}^{-1}$, in order of decreasing amplitude. Changes in the prewhitening procedure and how the additional stochastic low-frequency variability is handled is likely the reason for the change in extracted frequencies. The last two reported frequencies are a harmonic pair that are likely associated with the same physical process. Table B1 of DW22 reports that HD 269953 has six signals, with the $2.671\,\mathrm{d}^{-1}$ peak having the highest amplitude ($f_0$). The periodogram shows additional significant peaks that do not appear to have been considered by these works, some of which are of higher signal-to-noise (S/N) ratio than the extracted frequencies. Here we investigate the four signals from DW20, which includes $f_0$ and its subharmonic. Figure B1 in the arXiv version `2206.11917v3` of DW22 implies that they find that the previously-dominant 1.593 and $1.174\,\mathrm{d}^{-1}$ signals can be ascribed to other OGLE sources.

Higgins & Bell (2022) developed a method that utilizes the high frequency resolution of TESS to mitigate source confusion challenges caused by its low spatial resolution. They demonstrate that the amplitudes of observed variations (modeled as sinusoids) measured by each individual pixel is proportional to the flux from the variable source recorded by that pixel. The distribution of best-fit amplitudes can be fit with the TESS pixel response function (PRF) model (Bryson et al. 2010) to constrain the position of the variable star on the sky.

The localization method is implemented in an open-source Python package, `TESS_localize`,[1] that we use to localize the signals observed in the light curve of HD 269953. The code takes a TESS Target Pixel File and observed frequencies of variability as inputs, and returns a best-fit source location. For best results, `TESS_localize` users are encouraged to validate the quality of the output; we reject all results with fitted PRF amplitudes less than five times their reported uncertainties (insignificant detections) or a reduced $\chi^2 > 20$ for the fit (poor fit agreement; see discussion in Higgins & Bell 2022). If the localization with the pipeline aperture does not return a satisfactory result, we try again with the "autoaperture" convenience function. We let `TESS_localize` attempt to automatically determine an appropriate number of principal components to use to detrend the light curves.

[1] https://github.com/Higgins00/TESS-Localize

Besides the pair of harmonic signals, there is no reason to assume that all detected signals originate from a single source in the blended TESS photometry. We run the pair of harmonics through `TESS_localize` together and the two other signal frequencies individually. We attempt to localize these signals in each of 23 TESS sectors of two-minute-cadence data available between Sectors 1 and 39. Considering the fits that pass our quality criteria (the majority for each signal), each frequency of variation gets localized to a consistent but different location on the sky. All are well separated from the YSG by more than a pixel, with a fit precision of $\approx 0.1$ pix.

Figure 2 displays all the reliable source locations obtained by `TESS_localize` plotted over the TESS Sector 34 Target Pixel File (TPF) in the top panel. The position of HD 269953 on the TPF is indicated by the red star, while the target pixel mask used to extract the 2-min cadence light curve by the TESS Science Processing Operations Center (SPOC) pipeline is shown by the hatched yellow region. Average fit locations corresponding to each of the three independent frequencies are presented with white circles with three different fill colors, including their $3\,\sigma_{\mathrm{std}}$ as error bars. The average (RA, Dec) fit coordinate for the $1.593\,\mathrm{d}^{-1}$ signal shown in grey is (85.0370, -69.6726) in decimal degrees (23.7″ from the YSG). The $1.174\,\mathrm{d}^{-1}$ signal (pink) is centered on (85.0160, -69.6693), and the $1.335\,\mathrm{d}^{-1}$ and its harmonic $f_0$ (blue) are localized to (85.0197, -69.6638) degrees (43.2″ and 41.5″ from the YSG, respectively). Figure 2 also shows the locations of known Gaia sources down to a $G$-magnitude of 17.

The bottom panels of Figure 2 display the light curves and their periodograms extracted with different apertures, color-coded to match the outlined apertures in the example image. Details on how the light curves were extracted and normalized are given in Appendix B. The first row shows the light curve and periodogram from the TESS SPOC pipeline aperture; the three main signals are marked in the periodogram with dashed vertical lines. Restricting the aperture to the two pixels containing most of the light from the target HD 269953, the next row shows the same signals to be absent. Extracting light curves from the individual pixels containing the average `TESS_localize` fit locations for the three independent signals for the next three panels confirms where these signals are observed to be strongest. Different signals varying in amplitude differently across pixels is a telltale sign of blended variable light curves (Colman et al. 2017). It is clear that none of the signals reported for HD 269953 from DW20 originate from the YSG target.

## 3. LOCALIZING THE FYPS SIGNALS

As demonstrated in detail for the FYPS prototype HD 269953 above, we can use `TESS_localize` to fit the sky positions of signals reported to belong to FYPS pulsators. Most of the FYPS signals are only detectable with multiple sectors of data; since `TESS_localize` can only fit a source location in a single sector at a time, it cannot reliably localize such weak signals. For signals that are strong enough to be detected in individual sectors, multiple sectors of data enable multiple independent localizations of the same signals. Finding consistent source locations across multiple sectors verifies the reliability of the results, especially since images from different sectors are oriented differently on the sky. The $f_0$ value provided in Table B1 and B2 of DW22 is the frequency of the highest-amplitude peak that they associate with each star in their sample. We attempt to recover these $f_0$ signals to full precision following a similar prewhitening methodology.

For each YSG star, we downloaded the 2-min cadence SPOC light curves from the Mikulski Archive for Space Telescopes (MAST) for all available sectors using the `lightkurve` Python package. Following DW22 , we used the Pre-search Data Conditioned Simple Aperture Photometry (PDCSAP) flux light curves, which have been corrected for systematic trends, and divided the flux in each sector by its corresponding median before combining all available sectors. These light curves should be identical to the ones used by DW22. Subsequently, we changed the flux units to parts-per-thousand (ppt), centered the light curves around zero, and carried out an iterative prewhitening following a similar procedure adopted by Pedersen et al. (2021), where the highest S/N signals are removed first using publically available time series analysis Python packages from the IvS repository[2]. Except for HV 829, we limited the prewhitening to frequencies below $10\,\mathrm{d}^{-1}$ and stopped once $S/N < 4$. The resulting extracted frequency lists were filtered for close frequencies using the Loumos & Deeming (1978) resolution criterion of $2.5/T$, where $T$ is the length of the light curve. We crossmatched this final list of frequencies with the tabulated $f_0$ values from Table B1 and B2 of DW22, in order to recover the reported $f_0$ values to a higher precision.

In 3 out of 17 cases, we were unable to identify a significant periodogram peak within the Rayleigh limit ($1/T$) of the tabulated $f_0$ values. We also identify other signals that are arithmetically related to $f_0$ as either belonging to the same harmonic sequence or a set of combination frequencies. These signals are likely be physically associated with the same source, as it is unlikely for unrelated signals to fall within frequency bins that are related in these ways by chance given the high frequency resolution of TESS (finer than $0.003\,\mathrm{d}^{-1}$ for stars in the TESS continuous viewing zones). The crossmatched $f_0$ values and associated combination frequencies used for `TESS_localize` are listed in Table 1.

Of the fourteen stars for which we can confirm a significant peak at $f_0$, we obtain at least one fit meeting our quality criteria for six. Our interpretation of the results for these targets is provided below. We consider four of the localizations to be reliable, as supported by consistent fitted source locations across multiple sectors.

- **HD 269953** was analyzed in detail in Section 2. The $f_0$ signal and its subharmonic are offset from the YSG target by 41.5″. Localization of these signals met our reliability criteria in 22 out of 23 available sectors of TESS data.

- **HD 268687** returned good fits for 20 out of 25 sectors, all consistent with an average location of (72.7433, -69.4356) degrees, which is 20.5″ from the target, see Fig. 3. This position is most consistent with a known eclipsing binary, OGLE LMC-ECL-1544, with an orbital period of 2.169763 days (Graczyk et al. 2011), of which $f_0$ is the 6th harmonic.

- **HD 33579** has 12 sectors of TESS data available and `TESS_localize` reported a marginally significant result for only Sector 29. The data from that sector shows considerable systematic noise, which can confuse localizations, especially for such low-frequency signals that only complete a few cycles per sector. Combined with a lack of corroboration from other sectors, we interpret this single "good" fit as spurious.

- **HD 268946** returns three localizations that pass our initial quality criteria out of twelve; however, we reject them as spurious detections since they are found at inconsistent sky locations. Inspecting the light curves suggests that the fits are coupling to TESS systematics with similar timescales as the alleged signal.

- **HD 269787** data yield six good localizations out of ten available sectors of data, all at consistent sky locations. The source of the $f_0$ signal is centered on (83.6215,-66.9711) degrees on average, which is 31.5″ from the position of the YSG target, see Fig. 3. The reported signal can be uniquely ascribed to the object

[2] https://github.com/IvS-KULeuven/IvSPythonRepository

**Table 1.** List of frequencies used to carry out the source identification with `TESS_localize` for the 17 FYPS stars.

| TIC ID | Common name | $N_f^{\rm DW}$ | $f_0^{\rm DW}$ ($\rm d^{-1}$) | $N_f$ | freq. ($\rm d^{-1}$) | Combination |
|---|---|---|---|---|---|---|
| 29984014 | HD 268687 | 6 | 2.765 | 13 | $f_0 = 2.76526$ | |
| 31106686 | HD 33579 | 13 | 0.177 | 1 | $f_0 = 0.17713$ | |
| 31109182 | HD 268946 | 8 | 0.168 | 6 | $f_0 = 0.16846$ | |
| 179304909 | SK -69 99 | 2 | 0.292 | 5 | $f_0 = 0.29210$ | |
| 276863889 | HD 269787 | 2 | 0.909 | 9 | $f_0 = 0.90868$ | |
| 276864037 | HD 269781 | 13 | 0.072 | 3 | ... | |
| 276869010 | HD 269762 | 4 | 0.176 | 7 | $f_0 = 0.17614$ | |
| 277108449 | HD 269840 | 3 | 0.717 | 13 | $f_0 = 0.71703$ | |
| 279956577 | HD 269604 | 1 | 0.105 | 10 | $f_0 = 0.10522$ | |
| | | | | | $f_1 = 0.09012$ | |
| | | | | | $f_2 = 0.19419$ | $f_0 + f_1$ |
| 279957325 | CD-69 310 | 13 | 0.101 | 10 | $f_0 = 0.10070$ | |
| 391813303 | HD 269651 | 2 | 0.098 | 4 | $f_0 = 0.09828$ | |
| 391815407 | HD 269661 | 21 | 4.784 | 15 | ... | |
| 404850274 | HD 269953 | 6 | 2.671 | 21 | $f_0 = 2.67059$ | |
| 425083216 | HD 269723 | 2 | 2.374 | 6 | $f_0 = 2.37353$ | |
| 181043309 | HV 829 | 30 | 29.893 | 5 | ... | |
| 181446366 | [VA82] II-2 | 1 | 0.899 | 6 | $f_0 = 0.90173$ | |
| | | | | | $f_1 = 1.80015$ | $2\,f_0$ |
| 267547804 | BZ Tuc | 4 | 0.183 | 1 | $f_0 = 0.18212$ | |

NOTE—The TIC IDs of the stars are listed, followed by their common name. The first 14 stars are LMC targets, while the last three are from the SMC. The number of prewhitened frequencies identified by DW22 is denoted as $N_f^{\rm DW}$, while $f_0^{\rm DW}$ is the corresponding highest amplitude frequency that they recover and do not attribute to a contaminating star. $N_f$ is our number of prewhitened frequencies. The sixth column lists the closest frequency from our list of extracted frequencies that match with the corresponding $f_0^{\rm DW}$ within the Rayleigh limit, as well as related frequencies used in our `TESS_localize` analysis. Empty entries means that no frequencies matched with $f_0^{\rm DW}$ within the Rayleigh limit. For the stars with multiple frequencies listed, the last column denotes how they are related.

AL 327 (TIC 276863886), an emission-line star (Andrews & Lindsay 1964; Howarth 2013) not previously studied as a photometric variable.

- **BZ Tuc** has two sectors of data available, and its main reported signal can be uniquely localized to the target in both, see Fig. 3. Despite this, we doubt that this represents an independent pulsation frequency for this well-studied variable star, as we address in the Section 4.

## 4. CONCLUSIONS

Of the first five YSGs that DW20 used to argue the existence of a new FYPS class of pulsating variable star, DW22 attribute the variability of HD 269110 and HD 269902 to contaminants based on OGLE data (`TESS_localize` confirms). We have shown that the main signals from HD 269953 and HD 268687 also originate from other sources. DW22 found the $1.135\,\mathrm{day}^{-1}$ signal that DW20 identified as the strongest for the remaining candidate, HD 269840, to be caused by contamination, which we confirm with `TESS_localize`. The remaining variations in the light curve that DW22 associate with HD 269840 are too weak for `TESS_localize` to locate, but there is no reason to assume that they belong to the YSG in such a crowded part of the sky. While DW22 make a statistical argument that all claimed FYPS are unlikely to be caused by contamination, we argue that FYPS should not be considered a class of pulsating star until rapid pulsational variability can be uniquely associated with a YSG.

For BZ Tuc, `TESS_localize` does support that the $0.182123\,\mathrm{d}^{-1}$ variation is intrinsic to the target. In this case, no other *Gaia* sources are consistent with the fit location, so the signal can be uniquely pinned to BZ Tuc. This is a fairly well studied Cepheid variable with one of the longest known periods of 127 days (as HV 821, e.g., Gascoigne & Kron 1965; Eggen 1977). We presume that the identified signal from TESS data may be a high harmonic of this known non-sinusoidal variation. In general, it is difficult to reliably measure intrinsic periods of variation close to or exceeding the TESS orbital period of 13.7 days, as this is a typical timescale of TESS systematics, and TESS light curves show significant systematic differences in flux zero points between sectors. This limitation of the TESS data has been borne out in efforts to measure stellar rotation periods (Canto Martins et al. 2020; Avallone et al. 2022; Holcomb et al. 2022).

This work demonstrates how much of a challenge source confusion can be for analyses of TESS data. While we focused here on the FYPS stars as a case study, it is not uncommon in the literature to analyze only pipeline-extracted TESS light curve products from MAST without inspecting the pixel data for contamination (we have done this ourselves, e.g., Pedersen et al. 2019; Bell et al. 2019). Even if contamination of the aperture is predicted to be low (estimated by the `CROWDSAP` header value), significant signals can still be caused by source blending (Higgins & Bell 2022). Though it takes more work, interrogating TESS data at the pixel level for contamination issues is essential if misattribution of signals is to be avoided; the `lightkurve` Python package can help to make the pixel data more accessible (Lightkurve Collaboration et al. 2018). Statistical arguments for the likelihood of contamination of TESS light curves may not be reliable. For localizing (multi-)periodic sinusoidal variability to sub-pixel precision, the Python tool `TESS_localize` can help in many cases (for guidance, see Higgins & Bell 2022).

The authors are grateful to Jim Fuller, Lars Bildsten, Tim Bedding, Conny Aerts, and Trevor Dorn-Wallenstein for their valuable discussions and comments at different stages of the manuscript. This research was supported in part by the National Science Foundation under Grant No. NSF PHY-1748958 as well as through the TESS Guest Investigator program Cycle 4 under Grant No. 80NSSC22K0743 from NASA and by the Professor Harry Messel Research Fellowship in Physics Endowment, at the University of Sydney. This research made use of Lightkurve, a Python package for Kepler and TESS data analysis (Lightkurve Collaboration et al. 2018). This paper includes data collected with the TESS mission, obtained from the MAST data archive at the Space Telescope Science Institute (STScI). Funding for the TESS mission is provided by the NASA Explorer Program. STScI is operated by the Association of Universities for Research in Astronomy, Inc., under NASA contract NAS 5–26555. This research has made use of the VizieR catalogue access tool, CDS, Strasbourg, France. This work has made use of data from the European Space Agency (ESA) mission *Gaia* (https://www.cosmos.esa.int/gaia), processed by the *Gaia* Data Processing and Analysis Consortium (DPAC, https://www.cosmos.esa.int/web/gaia/dpac/consortium). Funding for the DPAC has been provided by national institutions, in particular the institutions participating in the *Gaia* Multilateral Agreement.

*Facilities:* TESS (Ricker et al. 2014), Gaia (Gaia Collaboration et al. 2016, 2022; Babusiaux et al. 2022)

*Software:* `astropy` (Astropy Collaboration et al. 2013, 2018), `TESS_localize` (Higgins & Bell 2022), `lightkurve` (Lightkurve Collaboration et al. 2018), `astroquery` (Ginsburg et al. 2019), `tesscut` (Brasseur et al. 2019), `numpy` (Harris et al. 2020), `matplotlib`

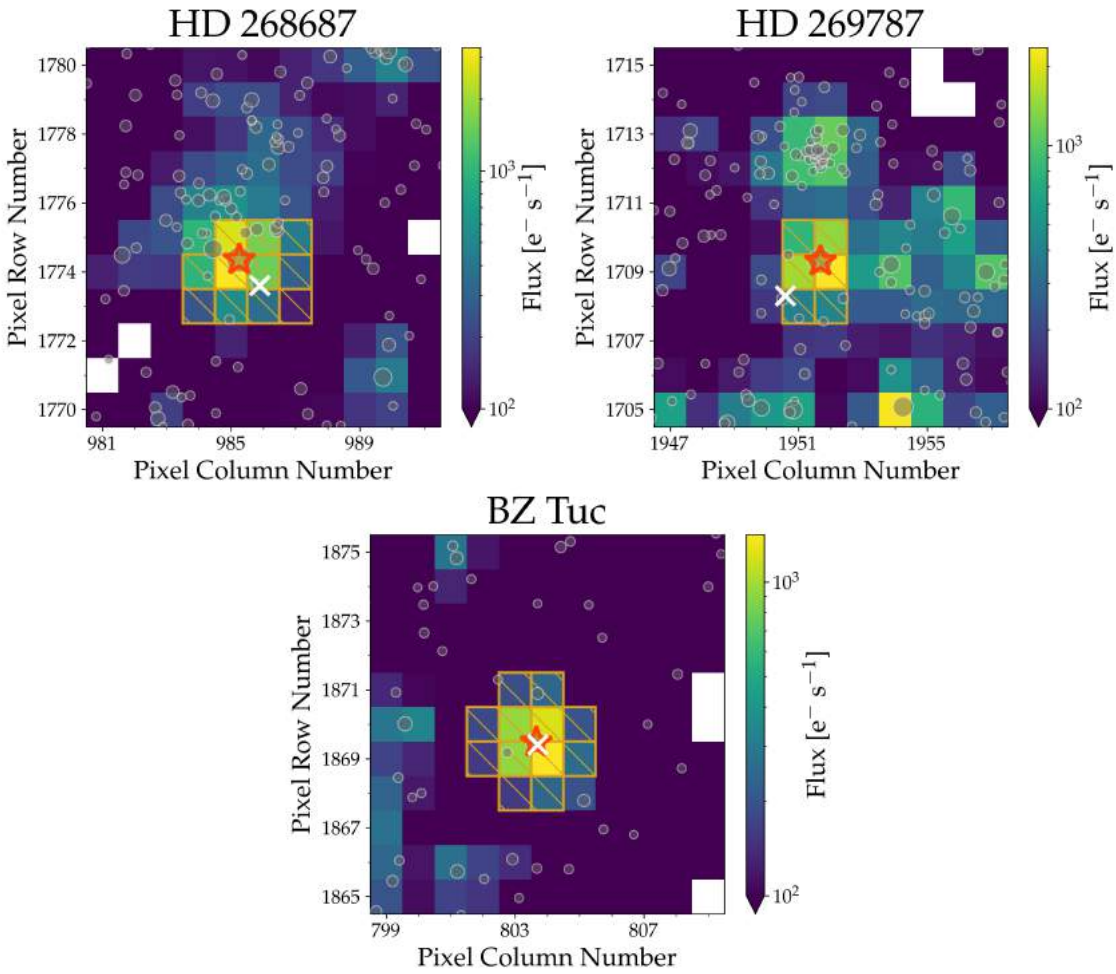


**Figure 3.** TESS localization results for three of the FYPS stars where the source of the variability could be unambiguously identified. The position of the target star is shown by the red star, while the position of the source of variability is indicated by the white cross. Positions of nearby Gaia sources brighter than 17 mag are also shown.

(Hunter 2007), `pandas` (pandas development team 2020; Wes McKinney 2010), `MESA` (Paxton et al. 2011, 2013, 2015, 2018, 2019; Jermyn et al. 2022).

## APPENDIX

### A. `MESA` SETUP

For the construction of Fig. 1 we computed non-rotating stellar evolution tracks for five different initial stellar masses ($15\,M_\odot$, $20\,M_\odot$, $25\,M_\odot$, $30\,M_\odot$, $35\,M_\odot$) using the stellar structure and evolution code `MESA` version 22.11.1 (Paxton et al. 2011, 2013, 2015, 2018, 2019; Jermyn et al. 2022). The models were evolved from the Hayashi track to the end of core He burning, assuming an initial stellar mass fraction for hydrogen, helium, and metals of $X = 0.7391$, $Y = 0.2562$, and $Z = 0.0047$ for the LMC following Köhler et al. (2015), who based these values on the observed abundances of young massive stars in the LMC (Brott et al. 2011). The Asplund et al. (2009) metal mixture and corresponding OP opacity tables were adopted. We used the Ledoux criterion with time-dependent convection, and adopted a small amount of convective boundary mixing following the exponential diffusive overshoot formalism (Freytag et al. 1996; Herwig 2000). Finally, we included mass loss from the Vink et al. (2001) hot wind scheme assuming a scaling factor of 0.3 (Björklund et al. 2021). The full `MESA` inlist will be made available online.

## B. LIGHT CURVE EXTRACTION AND CORRECTION FOR THE HD 269953 EXAMPLE

The light curves and associated periodograms shown in Fig. 2 were obtained in two different ways. For the SPOC target pixel mask indicated by the hatched yellow region in the top panel of the figure, we downloaded the SPOC 2-min cadence PDCSAP flux light curve from MAST using the `lightkurve` Python package. The downloaded light curve was subsequenctly normalized by dividing by the median flux of the sector, and the flux units changed to parts-per-thousand (ppt). Finally, the light curve is centered around zero and the Lomb-Scargle periodogram calculated. These median normalized SPOC PDCSAP flux light curves correspond to the ones analyzed by Dorn-Wallenstein et al. (2019, 2020, 2022).

For the remaining four pixel masks, the light curves were extracted and corrected manually once again relying on `lightkurve` and its `RegressionCorrector` class. The four light curves were extracted using simple aperture photometry for the selected target pixel mask of HD 269953 (red) and three pixel masks for the three contaminating stars shown in grey, pink, and blue in Fig. 2. The background flux was extracted by creating a background pixel mask, where all pixels fainter than 0.001 times the standard deviation above the overall median flux in the TPF were included. To subsequently reduce the dimensionality of the design matrix of the background flux used for the linear regression, a principal component analysis was performed where the dominant flux variability of the background pixels were captured using up to five principal components.

Using the constructed design matrix, the extracted target and contaminator light curves are corrected by creating a model of the background flux using linear regression and subtracting the model from the uncorrected light curves. Finally, the corrected light curves are normalized using a low order polynomial and centered around zero after changing the flux units to ppt. The final light curves and associated periodograms for Sector 34 are shown in the six bottom panels of Fig. 2.

## REFERENCES


Andrews, A. D., & Lindsay, E. M. 1964, Irish Astronomical Journal, 6, 241

Asplund, M., Grevesse, N., Sauval, A. J., & Scott, P. 2009, ARA&A, 47, 481, doi: 10.1146/annurev.astro.46.060407.145222

Astropy Collaboration, Robitaille, T. P., Tollerud, E. J., et al. 2013, A&A, 558, A33, doi: 10.1051/0004-6361/201322068

Astropy Collaboration, Price-Whelan, A. M., Sipőcz, B. M., et al. 2018, AJ, 156, 123, doi: 10.3847/1538-3881/aabc4f

Avallone, E. A., Tayar, J. N., van Saders, J. L., et al. 2022, ApJ, 930, 7, doi: 10.3847/1538-4357/ac60a1

Babusiaux, C., Fabricius, C., Khanna, S., et al. 2022, arXiv e-prints, arXiv:2206.05989. https://arxiv.org/abs/2206.05989

Bell, K. J., Córsico, A. H., Bischoff-Kim, A., et al. 2019, A&A, 632, A42, doi: 10.1051/0004-6361/201936340

Björklund, R., Sundqvist, J. O., Puls, J., & Najarro, F. 2021, A&A, 648, A36, doi: 10.1051/0004-6361/202038384

Brasseur, C. E., Phillip, C., Fleming, S. W., Mullally, S. E., & White, R. L. 2019, Astrocut: Tools for creating cutouts of TESS images. http://ascl.net/1905.007

Brott, I., Evans, C. J., Hunter, I., et al. 2011, A&A, 530, A116, doi: 10.1051/0004-6361/201016114

Bryson, S. T., Tenenbaum, P., Jenkins, J. M., et al. 2010, ApJL, 713, L97, doi: 10.1088/2041-8205/713/2/L97

Canto Martins, B. L., Gomes, R. L., Messias, Y. S., et al. 2020, ApJS, 250, 20, doi: 10.3847/1538-4365/aba73f

Colman, I. L., Huber, D., Bedding, T. R., et al. 2017, MNRAS, 469, 3802, doi: 10.1093/mnras/stx1056

Dorn-Wallenstein, T. Z., Levesque, E. M., & Davenport, J. R. A. 2019, ApJ, 878, 155, doi: 10.3847/1538-4357/ab223f

Dorn-Wallenstein, T. Z., Levesque, E. M., Davenport, J. R. A., et al. 2022, arXiv e-prints, arXiv:2206.11917. https://arxiv.org/abs/2206.11917

Dorn-Wallenstein, T. Z., Levesque, E. M., Neugent, K. F., et al. 2020, ApJ, 902, 24, doi: 10.3847/1538-4357/abb318

Eggen, O. J. 1977, ApJS, 34, 1, doi: 10.1086/190441

Freytag, B., Ludwig, H. G., & Steffen, M. 1996, A&A, 313, 497

Gaia Collaboration, Prusti, T., de Bruijne, J. H. J., et al. 2016, A&A, 595, A1, doi: 10.1051/0004-6361/201629272

Gaia Collaboration, Vallenari, A., Brown, A. G. A., et al. 2022, arXiv e-prints, arXiv:2208.00211. https://arxiv.org/abs/2208.00211

Gascoigne, S. C. B., & Kron, G. E. 1965, MNRAS, 130, 333, doi: 10.1093/mnras/130.5.333

Ginsburg, A., Sipőcz, B. M., Brasseur, C. E., et al. 2019, AJ, 157, 98, doi: 10.3847/1538-3881/aafc33

Graczyk, D., Soszyński, I., Poleski, R., et al. 2011, AcA, 61, 103. https://arxiv.org/abs/1108.0446

Harris, C. R., Millman, K. J., van der Walt, S. J., et al. 2020, Nature, 585, 357, doi: 10.1038/s41586-020-2649-2

Herwig, F. 2000, A&A, 360, 952. https://arxiv.org/abs/astro-ph/0007139

Higgins, M. E., & Bell, K. J. 2022, arXiv e-prints, arXiv:2204.06020. https://arxiv.org/abs/2204.06020

Holcomb, R. J., Robertson, P., Hartigan, P., Oelkers, R. J., & Robinson, C. 2022, ApJ, 936, 138, doi: 10.3847/1538-4357/ac8990

Howarth, I. D. 2013, A&A, 555, A141, doi: 10.1051/0004-6361/201321857

Hunter, J. D. 2007, Computing in Science & Engineering, 9, 90, doi: 10.1109/MCSE.2007.55

Jermyn, A. S., Bauer, E. B., Schwab, J., et al. 2022, arXiv e-prints, arXiv:2208.03651. https://arxiv.org/abs/2208.03651

Köhler, K., Langer, N., de Koter, A., et al. 2015, A&A, 573, A71, doi: 10.1051/0004-6361/201424356

Lightkurve Collaboration, Cardoso, J. V. d. M., Hedges, C., et al. 2018, Lightkurve: Kepler and TESS time series analysis in Python, Astrophysics Source Code Library. http://ascl.net/1812.013

Loumos, G. L., & Deeming, T. J. 1978, Ap&SS, 56, 285, doi: 10.1007/BF01879560

pandas development team, T. 2020, pandas-dev/pandas: Pandas, latest, Zenodo, doi: 10.5281/zenodo.3509134

Paxton, B., Bildsten, L., Dotter, A., et al. 2011, ApJS, 192, 3, doi: 10.1088/0067-0049/192/1/3

Paxton, B., Cantiello, M., Arras, P., et al. 2013, ApJS, 208, 4, doi: 10.1088/0067-0049/208/1/4

Paxton, B., Marchant, P., Schwab, J., et al. 2015, ApJS, 220, 15, doi: 10.1088/0067-0049/220/1/15

Paxton, B., Schwab, J., Bauer, E. B., et al. 2018, ApJS, 234, 34, doi: 10.3847/1538-4365/aaa5a8

Paxton, B., Smolec, R., Schwab, J., et al. 2019, ApJS, 243, 10, doi: 10.3847/1538-4365/ab2241

Pedersen, M. G., Chowdhury, S., Johnston, C., et al. 2019, ApJL, 872, L9, doi: 10.3847/2041-8213/ab01e1

Pedersen, M. G., Aerts, C., Pápics, P. I., et al. 2021, Nature Astronomy, 5, 715, doi: 10.1038/s41550-021-01351-x

Ricker, G. R., Winn, J. N., Vanderspek, R., et al. 2014, in Society of Photo-Optical Instrumentation Engineers (SPIE) Conference Series, Vol. 9143, Space Telescopes and Instrumentation 2014: Optical, Infrared, and Millimeter Wave, ed. J. Oschmann, Jacobus M., M. Clampin, G. G. Fazio, & H. A. MacEwen, 914320, doi: 10.1117/12.2063489

Saio, H., Georgy, C., & Meynet, G. 2013, MNRAS, 433, 1246, doi: 10.1093/mnras/stt796

Udalski, A., Szymański, M. K., & Szymański, G. 2015, AcA, 65, 1. https://arxiv.org/abs/1504.05966

Vink, J. S., de Koter, A., & Lamers, H. J. G. L. M. 2001, A&A, 369, 574, doi: 10.1051/0004-6361:20010127

Wes McKinney. 2010, in Proceedings of the 9th Python in Science Conference, ed. Stéfan van der Walt & Jarrod Millman, 56 – 61, doi: 10.25080/Majora-92bf1922-00a